HHS Public Access

Author manuscript

Cell Host Microbe. Author manuscript; available in PMC 2017 June 08.

Published in final edited form as:

Cell Host Microbe. 2016 June 8; 19(6): 826–836. doi:10.1016/j.chom.2016.05.007.

The response of *Acinetobacter baumannii* to Zinc starvation

Brittany L. Nairn[1], **Zachery R. Lonergan**[1], **Jiefei Wang**[2], **Joseph J. Braymer**[2], **Yaofang Zhang**[3,5], **M. Wade Calcutt**[3,5], **John P. Lisher**[2], **Benjamin A. Gilston**[4], **Walter J. Chazin**[4,5,6], **Valerie de Crécy-Lagard**[7], **David P. Giedroc**[2,#], and **Eric P. Skaar**[1,8,#]

[1]Department of Pathology, Microbiology, and Immunology, Vanderbilt University School of Medicine, Nashville, TN, 37232, USA

[2]Department of Chemistry, Indiana University, Bloomington, IN, 47405, USA

[3]Mass Spectrometry Research Center, Vanderbilt University School of Medicine, Nashville, TN, 37232, USA

[4]Center for Structural Biology, Vanderbilt University School of Medicine, Nashville, TN, 37232, USA

[5]Department of Biochemistry, Vanderbilt University School of Medicine, Nashville, TN, 37232, USA

[6]Department of Chemistry, Vanderbilt University, Nashville, TN, 37232, USA

[7]Department of Microbiology and Cell Science, University of Florida, Gainesville, FL, 32611, USA

[8]Tennessee Valley Healthcare Systems, US Department of Veterans Affairs, Nashville, TN, 37232 USA

Summary

Zinc (Zn) is an essential metal that vertebrates sequester from pathogens to protect against infection. Investigating the opportunistic pathogen *Acinetobacter baumannii's* response to Zn starvation, we identified a putative Zn metallochaperone, ZigA, which binds Zn, is required for bacterial growth under Zn-limiting conditions, and for disseminated infection in mice. ZigA is encoded adjacent to the histidine (His) utilization (Hut) system. The His ammonia-lyase HutH, binds Zn very tightly only in the presence of high His and makes Zn bioavailable through His catabolism. The released Zn enables *A. baumannii* to combat host-imposed Zn starvation. These

[#]Corresponding authors, Eric P. Skaar, PhD, MPH, Department of Pathology, Microbiology, and Immunology, Vanderbilt University School of Medicine, A5102 MCN, 1161 21st Avenue South, Nashville, TN 37232-2363 USA, Tel: 615-343-0002, Fax: 615-343-7392, eric.skaar@vanderbilt.edu, David P. Giedroc, PhD, Department of Chemistry, Indiana University, 800 E. Kirkwood Avenue, Bloomington, IN 47405-7102 USA, Tel: 812-856-3178, Fax: 812-856-5710, giedroc@indiana.edu.

Author Contributions

E.P.S., D.P.G., and B.L.N. conceptualized and designed the study. B.L.N., E.P.S., and D.P.G. wrote the manuscript. B.G. and W.J.C. produced and provided recombinant CP and S100A12. M.W.C., Z.R.L., and B.L.N. performed the metabolite mass spectrometry experiments. B.L.N., Z.R.L., J.P.L. and Y.Z. performed ICP-MS experiments. J.W., J.J.B., and B.L.N. performed the metal-binding experiments and J.W. carried out all enzyme assays. V.d.C-L. performed the genomic analyses of ZigA paralogs. Z.R.L. and B.L.N. performed the remaining experiments. All authors provided comments on the manuscript.

results demonstrate that *A. baumannii* employs several mechanisms to ensure bioavailability of Zn during infection, with ZigA functioning predominately during Zn starvation, but HutH operating in both Zn deplete and replete conditions to mobilize a labile His-Zn pool.

Graphical abstract

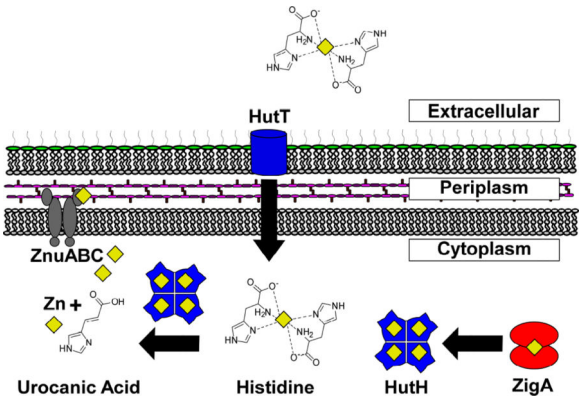

Introduction

Zn is required for all life, functioning as a catalyst for enzymatic reactions, a Lewis acid, and a structural cofactor for proteins. It is estimated that at least 10% of the eukaryotic proteome and 6% of the *Escherichia coli* proteome binds Zn (Andreini et al., 2006; Waldron et al., 2009). Conversely, excess Zn can result in mis-metallation of non-Zn binding proteins and subsequent toxicity (Imlay, 2015). Therefore, cells tightly regulate Zn levels to balance the essentiality of Zn against its toxicity at high concentrations.

Once inside the cell, Zn must exist in a bioavailable form for delivery to Zn-binding proteins and sensing by Zn metalloregulators. *Saccharomyces cerevisiae* stores Zn in vacuoles by distinct mechanisms depending on the cellular Zn status (Simm et al., 2007). In eukaryotes and a few cyanobacteria, metallothionein chelates Zn intracellularly to buffer toxic Zn levels (Bruins et al., 2000; Palacios et al., 2011). In bacteria that lack metallothionein, glutathione or bacillithiol can buffer Zn (Helbig et al., 2008; Ma et al., 2014). These factors sequester Zn to prevent toxicity and provide Zn for use as cofactors by newly synthesized proteins. Despite these examples, the nature of the labile Zn pool in most cells remains poorly defined, nor is it known how cells access this pool for distribution to Zn-binding proteins (Cavet et al., 2015; Loutet et al., 2015). For metals such as iron, nickel (Ni), and cobalt (Co), metallocenter formation is executed by at least one metallochaperone and often accessory proteins. Metallation of some Zn proteins may also require a metallochaperone, although none has thus far been identified. Strong candidates are found within the G3E GTPase protein family, some of which are clearly involved in metalloenzyme maturation by an activating metal or metallocofactor (Padovani and Banerjee, 2009; Soriano et al., 2000). COG0523 proteins represent one of four subfamilies of G3E GTPases (Haas et al., 2009), and are predicted to function as magnesium (Mg)- and Zn-binding metallochaperones. Little support for this hypothesis is available, and target proteins have not been identified. COG0523 orthologs are found across Kingdoms including some described in *Acinetobacter*

sp., E. coli, Bacillus subtilis, Clamydomonas reinhardtii, Arabidopsis thaliana, and *Homo sapiens* (Haas et al., 2009). Three COG0523 subfamily members have been studied, including YeiR and YjiA in *E. coli* and YciC in *B. subtilis*, yet the functions of these proteins are unknown (Blaby-Haas et al., 2012; Gabriel et al., 2008; Sydor et al., 2013).

During infection, pathogens must acquire nutrient metals, including Zn, from the vertebrate host. Vertebrates in turn defend against microbial invaders through metal sequestration in a process known as nutritional immunity (Hood and Skaar, 2012). The vertebrate Zn- and manganese (Mn)-chelating protein calprotectin (CP, S100A8/S100A9 heterodimer) is recruited to sites of infection to restrict nutrient access and inhibit microbial growth (Corbin et al., 2008). Therefore, in order to survive, bacterial pathogens have strategies to combat CP-dependent Zn and Mn sequestration. *A. baumannii* is a Gram-negative, opportunistic pathogen that is a significant cause of infection in hospitals worldwide, particularly as a leading cause of ventilator-associated pneumonia (Doyle et al., 2011). CP inhibits *A. baumannii* growth and protects against *A. baumannii* infection in a mouse model of pneumonia (Hood et al., 2012). In response to CP, *A. baumannii* up-regulates the expression of the inner membrane, high affinity Zn importer ZnuABC, required for adaptation to host-imposed Zn starvation. Loss of *znuB* results in reduced survival in the presence of CP *in vitro* and *in vivo* in a mouse model of pneumonia (Hood et al., 2012).

In *A. baumannii*, the transcriptional response to CP-induced Zn starvation is mediated by Zur (Zn uptake repressor) (Mortensen et al., 2014). Zur not only regulates *znuABC*, but also genes encoding for proteins involved in Zn homeostasis. Upon exposure to CP or loss of *zur* (Δ*zur*), the most highly expressed *A. baumannii* gene is *A1S_3411*, annotated as a G3E (COG0523) GTPase that we have named *zigA* (Zur-induced GTPase A). The promoter of *zigA* harbors a Zur box sequence, and *zigA* is directly regulated by Zur (Mortensen et al., 2014). In this work we show that ZigA binds Zn, exhibits GTPase activity, and is required for full growth in Zn-limiting conditions. In addition, we demonstrate that ZigA is encoded adjacent to the His utilization (Hut) system, and that strains lacking *zigA* have increased levels of intracellular His, are defective for growth in His as a sole carbon source, and have increased resistance to Zn toxicity, implicating His as part of the labile Zn pool in *A. baumannii*. We also show that the His ammonia-lyase (HAL), HutH, has an affinity for Zn that approaches that of ZigA, but only in the presence of substrate His, in a catalytically competent fashion. These results are consistent with a model whereby ZigA functions as a metallochaperone required for HutH degradation of His, which is maximally active under conditions of high His and low bioavailable Zn. This leads to the liberation of a labile Zn pool that enables *A. baumannii* to grow in the Zn-limiting conditions of the vertebrate host.

Results

ZigA contributes to *A. baumannii* growth during host-imposed Zn starvation

The up-regulation of *zigA* following exposure to CP led us to investigate the contribution of ZigA to the *A. baumannii* response to Zn starvation. ZigA expression was first evaluated in response to the Zn chelators TPEN or CP by immunoblotting for ZigA in *A. baumannii* lysates in wild-type (WT) or a *zigA* deletion strain (Δ*zigA*), and revealed that ZigA is more abundant in Zn-limiting conditions (Figure 1A). To evaluate the requirement for ZigA

during the *A. baumannii* response to Zn starvation, the growth of Δ*zigA* was compared to that of WT in the presence of CP or the S100A12 homodimer, a known Zn and Cu chelator (Haley et al., 2015). Δ*zigA* has a reduced growth rate compared to WT in the presence of CP (Figure 1B, S1A) or S100A12 (Figure 1C, S1B), and growth is restored by the addition of Zn, indicating that the growth inhibition is due specifically to Zn limitation (Figure 1B, C). Furthermore, the Δ*zigA* growth defect can be complemented by expressing *zigA in trans* (Figure 1D).

We next assessed the role of ZigA in a mouse model of *A. baumannii* pneumonia in WT and CP-deficient mice (S100A9$^{-/-}$). Although there were no differences in bacterial burdens of WT or Δ*zigA* recovered from the lungs of WT or S100A9$^{-/-}$ mice (Figure 1E), Δ*zigA* is attenuated in its ability to disseminate to the liver (Figure 1F). In CP-deficient mice, the liver burdens of Δ*zigA* were statistically indistinguishable from WT bacterial burdens, demonstrating that the defect is affected by the presence of CP (Figure 1F). These data establish that ZigA contributes to *A. baumannii* adaptation to Zn starvation and to dissemination during infection.

ZigA belongs to the conserved COG0523 subfamily of G3E GTPases

ZigA contains the signature motifs of the COG0523 subfamily in the N-terminus: the two Walker box motifs, the metal-binding motifs, and the NKxD GTPase domain (Figure 2A). The C-terminal regions of COG0523 proteins are hypervariable (Haas et al., 2009), and the proteins of the ZigA subset harbor strictly conserved tryptophan residues in this region (Figure 2A). Phylogenetic analyses group ZigA with *Acinetobacter baylyi* sp. ADP1 protein ACIAD1741 (Figure 2B), a member of COG0523 subgroup 1 that is also regulated by Zur (Figure 2C) (Haas et al., 2009). Of note, a second COG0523 family member, A1S_0934, and its homologs are found within sequenced *A. baumannii* strains in different gene contexts and do not conserve ZigA-like C-terminal features, and thus are more distantly related to ZigA (Figure 2B). Moreover, *A1S_0934* is not Zur-regulated (Mortensen et al., 2014) nor up-regulated in the presence of CP (Figure 2E).

The *A. baumannii* Hut system is encoded adjacent to *zigA* and predicted to consist of a putative importer, HutT, and enzymes responsible for the breakdown of *L*-His to *L*-glutamate: HutH, HutU, HutI, and HutG. HutH is a candidate HAL responsible for the conversion of *L*-His to *trans*-urocanic acid through the removal of the α-amino group (Figure 2D) (Bender, 2012). HutU then hydrates *trans*-urocanic acid to imidazolone propionate, which is cleaved to formiminoglutamate (FG) by HutI. Finally, HutG hydrolyzes FG to produce formamide and *L*-glutamate (Figure 2D). Some organisms, including *A. baumannii*, encode HutD within the locus, but HutD has no defined function (Zhang and Rainey, 2007). HutC, a transcriptional regulator of the *hut* system, is regulated by urocanic acid levels, nitrogen levels, and catabolite repression, with candidate HutC binding sites found in *A. baumannii* upstream of the *hutC* and *hutU* genes (Figure 2C). These analyses categorize ZigA into the COG0523 subfamily and suggest that a potential target for ZigA lies within the Hut cluster.

ZigA is a GTPase that binds Zn with high affinity

In order to test the GTPase activity of ZigA, we used recombinant ZigA in a Malachite green assay, which quantifies inorganic phosphate release. The GTPase activity of ZigA measured as a function of GTP concentration is low and increases in the presence of Zn. The apparent K_m for Zn-ZigA is 150 μM GTP, with a turnover number, k_{cat}, of 0.002 s^{-1} (Figure 3A; Figure S2A, B). These kinetic parameters are consistent with those described for other G3E members: low GTP hydrolysis in the absence of client proteins (Blaby-Haas et al., 2012; Maier et al., 1993; Sydor et al., 2013; Zambelli et al., 2005).

Given the Zn-dependent stimulation of GTPase activity, the metal binding properties and nucleotide-dependent assembly state changes in ZigA were measured. Inductively-coupled plasma mass spectrometry (ICP-MS) analysis revealed significant association of Mg and Zn with purified ZigA (Figure 3B). Next, metal-free apo-ZigA was subjected to Co-binding (Figure S2C–E) and chelator competition experiments in which Zn is titrated into a mixture of ZigA and fluorescent chelators of known Zn affinity, including mag-fura-2 (mf2), quin-2, or 4-(2-pyridylazo)resorcinol (PAR) (Figure 3C; Figure S2F, G). Co(II) is often used a spectroscopic surrogate for Zn, due to its favorable visible electronic absorption properties (VanZile et al., 2002). These results reveal that a single molar equivalent of Co binds to a cysteine sulfur-rich site with a coordination number of 4–5, consistent with previous work on *E. coli* YjiA (Figure S2C–E) (Sydor et al., 2013). Zn chelator competition experiments show a stoichiometry of two Zn per ZigA protomer (subunit), with one high affinity ($K_{Zn1} \approx 10^{11}$ M^{-1}) and one lower affinity ($K_{Zn2} \approx 10^{7}$ M^{-1}) site (Figure 3C; Figure S2F, G). Gel permeation chromatography reveals that apo-ZigA is dimeric, and addition of up to 3 molar equivalents of Zn has no impact on this assembly state (Figure 3D). However, addition of 3 mM Mg•GDP to Zn-ZigA begins to shift this dimeric state to that consistent with an asymmetric monomer. GTP and the non-hydrolyzable GTP analog, GDPNP, strongly shifts the equilibrium toward monomer. Taken together, these data show that ZigA is a Mg- and Zn-binding GTPase that binds Zn with high affinity, and that Mg•GTP shifts the dimeric assembly state of ZigA to that of a monomer.

HutH is a Zn-binding HAL required for growth in low Zn

To determine if the *hut* system is up-regulated in response to Zn starvation, the expression of *hutH, hutU, hutI*, and *hutG* were evaluated by qRT-PCR during CP treatment (Figure 4A) or in the presence of excess Zn (Figure S3A). Each gene exhibits increased expression during CP exposure but not under conditions of Zn excess, revealing that the Hut system is responsive to the cellular Zn status.

The activity of metal-free HALs from other sources can be stimulated by the addition of several divalent metals (Klee, 1972). We therefore tested the ability of recombinant *A. baumannii* HutH to bind Zn and stimulate its activity. Zn chelator competition experiments reveal that apo-HutH binds a single protomer mol•equiv of Zn with modest affinity relative to ZigA, $K_{Zn} = 5 \times 10^{6}$ M^{-1}, confirming that HutH binds Zn (Figure 4B). Further, HutH is a *bona fide* HAL whose specific activity is stimulated nearly 30-fold by Zn (Figure 4C), with half-maximal stimulation of the activity occurring at $\approx 10^{-10}$ M Zn (Figure 4D). Interestingly, Zn activation of tetrameric HutH HAL activity is highly cooperative under

these conditions (Figure 4D). The affinity of HutH for Zn is therefore ≈1000-fold greater in the presence of high *L*-His given the effective affinities measured in the absence (Figure 4B) and presence (Figure 4D) of *L*-His. Further, given their similar Zn affinities, HutH may effectively compete for Zn with ZigA under conditions of low Zn and high His, and as a result may be capable of utilizing ZigA-derived Zn for HAL activity (Figure 4C), although this is not established here. We could obtain no evidence that HutH and ZigA stably interact with one another (Figure S4). We conclude that HutH is a candidate target of ZigA-dependent Zn metallation, and suggest that *A. baumannii* may activate His degradation in response to Zn starvation via incorporation of Zn into HutH.

To assess whether HutH is required for growth during Zn starvation, a *hutH* deletion strain (Δ*hutH*) was grown in the presence of CP. Δ*hutH* exhibits decreased growth in the presence of CP relative to WT, a phenotype reversed by Zn supplementation or *in trans* complementation (Figure 4E, F, S3B). In contrast, the loss of *hutU* did not impact *A. baumannii* growth in the presence of CP (Figure S3C), consistent with the idea that it is *L*-His, and not urocanic acid, that limits Zn availability. These data demonstrate that HutH is required for *A. baumannii* adaptation to Zn starvation, linking HutH activity to Zn homeostasis.

ZigA and HutH are required for release of a His-Zn pool

Free His can coordinate Zn in exchange-labile complexes and impact metal homeostasis (Murphy et al., 2011), leading to the proposal that the labile Zn pool within cells may be buffered by free His. We hypothesized that during Zn starvation, HutH reduces the total concentration of the effective competitor ligand His, providing access to the Zn pool by Zn-dependent proteins, via simple mass action. HutH activity, in turn, may be activated by ZigA.

To test this model, we first compared the Zn affinities of the HutH substrate, *L*-His with the HutH product, *trans*-urocanic acid. A chelator competition was performed by titrating Zn into a mixture of *L*-His or urocanic acid and mf2 and optimized K_{Zn} for each small molecule using a 1:1 or 2:1 binding models (Figure S5A, B). These experiments show that *L*-His binds Zn with an 8-fold higher affinity than urocanic acid. Although the affinity of *L*-His for Zn (Ka≈10^5 M^{-1}; Figure S5A) is substantially weaker than typical Zn metalloproteins (Colvin et al., 2010), it is comparable to HutH in the absence of His (Figure 4B). In both Zn deplete and Zn replete conditions Δ*hutH* accumulates more intracellular *L*-His, whereas *L*-His levels are unaffected in Δ*hutU*, supporting that HutH catalysis is the rate-determining step in His degradation (Figure 5A, B). Importantly, *L*-His levels are increased in Δ*zigA* (Figure 5A, B), consistent with the proposal that HutH activity is stimulated by ZigA in low Zn (Figure 4C, D). These observations suggest that ZigA functions predominately during Zn starvation, but HutH operates in both Zn deplete and replete conditions.

If HutH and ZigA are required to liberate Zn from intracellular His pools, we hypothesized that the enzymes' activities may contribute to Zn toxicity during Zn excess. To test this hypothesis, WT, Δ*zigA*, and Δ*hutH* strains were grown in toxic levels of Zn. Both Δ*zigA* and Δ*hutH* display increased resistance to Zn toxicity compared to WT (Figure 5C, S5C). Strikingly, Δ*zigA* is characterized by rapid and enhanced resistance to Zn toxicity when

compared to Δ*hutH*, implying that ZigA may be impacting intracellular His and Zn levels in multiple ways (Figure 5C). To confirm that His can protect against Zn toxicity, either *L*-His or *D*-His was added to the cultures (Figure 5D). Both *L*-His and *D*-His improve the growth of all strains, albeit to a lesser degree for Δ*zigA*. The growth rescue is greater with *D*-His (not metabolized), indicating that the improved growth is due largely to Zn buffering. Together these data support a model where His buffers the cell against Zn toxicity and serves as a component of the labile Zn pool in *A. baumannii*.

Next, we assessed the effect of ZigA on HutH-mediated His degradation by measuring growth in *L*-His as a sole carbon source. As expected, in Zn-replete conditions, Δ*hutH* and Δ*hutU* cannot grow on *L*-His as a sole carbon source (see Figure 6C, below). This contrasts with Δ*zigA* which grows like WT, revealing that replete Zn bypasses the essentiality of ZigA in *L*-His catabolism. In Zn-deplete conditions on the other hand, Δ*zigA* is inhibited for growth on *L*-His whereas WT and Δ*zur* are not (Figure 5E). Further, Δ*hutH* has increased levels of His and resistance to Zn toxicity (Figure 5A–D), demonstrating that ZigA directly affects intracellular His pools and utilization specifically under low Zn conditions. These data are consistent with a model whereby ZigA is required for HutH activity in low Zn, and that HutH-dependent His degradation mobilizes a Zn pool that enables *A. baumannii* to survive Zn starvation.

We next investigated whether ZigA or HutH impact Zn levels in the cell. Intracellular Zn concentrations were measured by ICP-MS in WT, Δ*hutH*, and Δ*zigA* grown in the presence or absence of CP (Figure 5F). All CP-treated strains have higher intracellular Zn levels, with Δ*zigA* characterized by a ≈10-fold increase. Transcriptional analysis reveals that Zur-regulated Zn acquisition genes in all three strains are up-regulated upon CP treatment (Figure S5D); moreover, Δ*zigA* up-regulates Zur-regulated genes in the absence of CP (Figure 5G). These data suggest that Δ*zigA* is functioning as though Zn-starved (the Zur regulon is induced) despite accumulating more Zn than WT; this is consistent with the idea that this Zn may not be detected by Zur, perhaps as a result of sequestration by His. Alternatively, Zn-starved *A. baumannii* may acquire Zn very rapidly, leading to a period of Zn accumulation prior to the point where homeostasis is reached. We conclude ZigA is a key regulator of intracellular Zn concentration and speciation, and that the *A. baumannii* Zn acquisition systems can effectively compete with CP for Zn.

The HutT His importer alters the His-Zn pool

Besides catabolism, intracellular His levels could be altered by perturbations in His transport. The putative His importer in *A. baumannii*, HutT, is found within the *hut* operon. We therefore hypothesized that HutT may impact the His-Zn pool. To determine if HutT is involved in Zn homeostasis, a *hutT* deletion mutant (Δ*hutT*) was evaluated for growth in the presence of CP. Δ*hutT* exhibits reduced growth in the presence of CP (Figure 6A, S6A), and this reduction can be restored by metal supplementation (Figure S6B) or by providing *hutT in trans* (Figure 6B). Importantly, Δ*hutT* expresses Zur-regulated Zn transporter genes at a level similar to WT cells (Figure S6C). Furthermore, the growth of Δ*hutT* is dramatically reduced compared to WT and Δ*zigA* in media using *L*-His as a sole carbon source indicating that HutT is the predominant His transporter in *A. baumannii* (Figure 6C). Compared to

Δ*zigA*, Δ*znuB*, and Δ*hutH*, Δ*hutT* exhibits decreased resistance to Zn toxicity, supporting the notion that His import is required for *A. baumannii* to buffer Zn (Figure 6D).

In order to assess the impact of CP-mediated Zn starvation on Zn import by *A. baumannii*, we measured isotopically labeled Zn (Zn^{70}) uptake following growth of WT and Δ*hutT* in the presence of CP by ICP-MS (Figure 6E). Zn uptake is increased during CP exposure that is diminished in Δ*hutT*, suggesting that HutT contributes to Zn uptake during Zn starvation. Finally, to determine if HutT is responsible for the uptake of His-Zn complexes, we assessed uptake of Zn^{70} in the absence or presence of *L*-His under conditions shown to result in His-Zn complex formation (Figure 6F). Compared to WT, Δ*hutT* shows a decrease in intracellular Zn^{70}, implicating HutT in the import of Zn-bound His. Overall, these data suggest that HutT impacts *A. baumannii* adaptation to Zn starvation through uptake of His-Zn complexes, thereby altering the labile Zn pool in the cell.

Discussion

This report presents the functional characterization of a Zur-regulated COG0523 protein in *A. baumannii* that we have named ZigA. We show that ZigA is a Zn-binding GTPase required for full growth in low Zn conditions and during infection. We also show that HutH is a Zn-activated HAL that cleaves His into urocanic acid. Both HutH and ZigA impact intracellular His levels and are required for His utilization during Zn starvation; further, ZigA may facilitate Zn binding by HutH, particularly under conditions of high His and low Zn. These findings are consistent with the designation of ZigA as a Zn metallochaperone. HutT, the His importer in *A. baumannii*, also impacts the His-Zn pool. These findings support a model positing that HutT imports His, which is a ligand in the labile Zn pool in *A. baumannii*. Upon Zn starvation, ZigA may facilitate the incorporation of Zn into HutH to stimulate His catabolism and resulting liberation of Zn stores from His chelation. Combined, these activities enable *A. baumannii* to combat Zn sequestration during infection.

For organisms that do not utilize low molecular weight thiols for Zn buffering, the labile Zn pool may be maintained by free amino acids (Cavet et al., 2015; Loutet et al., 2015). Here we provide evidence that His serves as a component of the labile Zn pool utilized by *A. baumannii* during conditions of both excess Zn (Figure 5) and low Zn (Figures 1, 4, 5, 6). Such a bimodal requirement reflects the necessity of a dynamic and labile Zn pool, which serves to chelate excess Zn and prevent toxicity, but is also bioavailable for activation of critical Zn-requiring proteins during Zn starvation. His-Zn complexes formed at neutral pH are $Zn(His)_2$, where Zn is bound at each amino group and one of the nitrogens in the imidazole side chain (Zhou et al., 2013). These studies support a model whereby cleavage of the amino group from His by HutH would release Zn from the $Zn(His)_2$ complex. Consistent with this model, His supplementation improves *C. elegans* survival in conditions of Ni or Zn toxicity, which is dependent on His metal binding (Murphy et al., 2011). This is similar to the alleviation of Zn toxicity in *A. baumannii* following His supplementation (Figure 5C–D). Relatedly, Zn-bound His can be actively transported into cells (Horn et al., 1995). We show that HutT is the predominant His importer in *A. baumannii* (Figure 6C). Importantly, Δ*hutT* has reduced growth in low Zn (Figure 6A, B, S6A, B), suggesting that His imported by HutT may be Zn-bound and contributing to the His-Zn pool.

Zn destined for Zn metalloproteins must originate from bioavailable Zn. Given the large number of Zn metalloenzymes in the cell, both passive and active processes are likely involved. An active process may require a metallochaperone for metallation of a number of Zn-requiring client enzymes, perhaps only under conditions of severe Zn starvation. We propose that ZigA functions in this way, either directly or indirectly through the activity of partner protein. ZigA is a G3E COG0523 subfamily GTPase, which have been implicated in metallocenter biogenesis (Padovani and Banerjee, 2009; Soriano et al., 2000; Sydor et al., 2011). ZigA binds Zn (Figure 3; Figure S2) and the activity of HutH, a candidate ZigA target, is stimulated by Zn (Figure 4). ZigA is a Zn-stimulated GTPase, like *E. coli* YeiR and YeiR, like ZigA, is required for growth in Zn-deplete conditions (Blaby-Haas et al., 2012; Sydor et al., 2013). This suggests that COG0523 members up-regulated under Zn limitation reallocate Zn into select Zn-requiring target proteins required to survive Zn starvation.

In summary, the response of *A. baumannii* to Zn starvation combines the deployment of a high affinity Zn transporter (Hood et al., 2012) with the liberation of a mobilizable pool of Zn bound to His. Liberation of Zn from His requires HutH-dependent His degradation, which may be activated by ZigA-facilitated Zn metallation. How HutH acquires Zn from ZigA, and the role of GTP hydrolysis in this process are unknown, as for other metallocenter assembly machines. It seems plausible that GTP binding, which stabilizes the monomeric form of Zn-ZigA (Figure 3), may expose a transient client protein interaction site. GTP hydrolysis may allow Zn to move from the high affinity site on ZigA to the active sites of the client, *e.g.*, HutH. His degradation by HutH may be coupled to ZigA activation. The combined activities of ZigA and HutH enable growth during Zn starvation and contribute to bacterial dissemination during *A. baumannii* infection. Taken together, these findings support the assignment of COG0523 members as metallochaperones, uncover His as a key cellular component of a labile Zn pool that can be accessed during Zn starvation, and establish His catabolism and ZigA as candidate targets for the development of new antimicrobials for the treatment of *A. baumannii* infection.

Experimental Procedures

Bacterial strains and reagents

Experiments were performed using *A. baumannii* ATCC 17978 or a mutant derivative. Cloning was performed in *E. coli* DH5α and protein expression in *E. coli* BL21 (DE3). Strains were cultured in Luria broth (LB) at 37 °C with aeration and OD_{600} used to measure bacterial growth unless noted. Kanamycin (Sigma) was used at 40 μg/mL. Ampicillin (Sigma) was used at 100 μg/mL for *E. coli* and 500 μg/mL for *A. baumannii*. Recombinant human CP and S100A12 were expressed and purified as previously described (Corbin et al., 2008; Haley et al., 2015).

Generation of deletion mutants and complementation vectors

The Δ*znuB* and Δ*zur* mutants are published (Hood et al., 2012; Mortensen et al., 2014). Strains inactivated for *zigA, hutH, hutU*, and *hutT* were generated as for Δ*zur*. Complementation vectors were made by cloning genes into pWH1266 vector as for Δ*zur* referenced above (see Supplemental Experimental Procedures).

Bacterial growth assays in TPEN

Overnight cultures of WT *A. baumannii*, mutants, and complementation strains were sub-cultured 1:50 in LB Amp500 for 1 h. Back-diluted cultures were then re-seeded 1:100 into LB containing 0–80 mM tetrakis-(2-pyridylmethyl)ethylenediamine (TPEN) and grown for 10 h.

Bacterial growth assays in CP and S100A12

Overnight cultures of *A. baumannii* strains were sub-cultured 1:50 in LB (or Amp500 for complementation) for 1 h and then diluted 1:100 into CP growth media, consisting of 40% CP buffer (20 mM Tris-HCl, pH 7.5, 100 mM NaCl, 5 mM β-mercaptoethanol, 3 mM $CaCl_2$) and 60% LB, to which was added 0–1000 mg/mL CP or S100A12, plus or minus 50 mM $ZnCl_2$, $MnCl_2$, or $CuCl_2$ and grown for 10 h.

Bacterial growth assays in high Zn

Overnight cultures of WT *A. baumannii* and mutant strains were grown in LB or LB Amp500 (complementation experiments) and then were diluted 1:100 into LB with 1.25 mM $ZnCl_2$ plus or minus 1 mM of *D*-His or *L*-His with growth monitored over time.

Bacterial growth in His

Overnight cultures of WT *A. baumannii* or mutant strains were sub-cultured 1:50 in LB for 1 h. Cultures were then diluted 1:100 in M9 Minimal Media (1X M9 salts, 2 mM $MgCl_2$, 0.1 mM $CaCl_2$, 1 mg/mL NH_4Cl, 1X Vishniac's trace metal mix (Vishniac, 1955) containing a titration of 0–50 mM acetate or 0–80 mM *L*-His. For low Zn, 50 mM acetate or 20 mM *L*-His was used and Vishniac's trace metal mix plus or minus Zn.

Mouse model of pneumonia

All of the animal infections were approved by the Vanderbilt University Institutional Animal Care and Use Committee. WT C57BL/6 mice were obtained from Jackson Laboratories, and $S100A9^{-/-}$ mice were a gift from Wolfgang Nacken. Nine-week-old mice were inoculated with a 1:1 mixture of WT *A. baumannii* and Δ*zigA* totaling 5×10^8 CFU of bacteria in 40 mL PBS. At 36 h post inoculation mice were euthanized, and CFU were enumerated in the lungs and livers following tissue homogenization and dilution plating on LB and LB Km40. The limit of detection of the assay is 200 CFU/g.

Protein expression in low Zn

Overnight cultures of WT *A. baumannii* or Δ*zigA* were sub-cultured 1:50 in LB for 1 h. These cultures were re-seeded 1:100 into CP growth media, plus or minus 250 mg/mL CP or into LB plus or minus 20 μM TPEN. After 2, 4, or 6 h of growth, cultures were pelleted at 4 °C. Pellets were suspended in 500 μL cold Lysis buffer (150 mM NaCl, 20 mM Tris-HCl, pH 7.5), transferred to Lysing Matrix B tubes (MP Biomedicals), and lysed using FastPrep-24 (MP) bead beater for 45 s at 6 m/s twice. Supernatants were transferred to fresh tubes, centrifuged 3 min to pellet debris, leaving the supernatant the whole cell lysate. Samples were analyzed by SDS-PAGE, transferred to nitrocellulose membranes, and blocked with 5% milk. Membranes were incubated with 1:10,000 rabbit anti-ZigA (see

Supplemental Experimental Procedures) followed by goat anti-rabbit Alexa Fluor® 680 1:10,000. Proteins were detected at 700 nm using the Odyssey Infrared Imaging System (LI-COR Biosciences).

Quantitative RT-PCR

Overnight cultures of WT or mutant *A. baumannii* were reseeded 1:50 in LB and grown for 1 h at 37 °C. These cultures were reseeded 1:100 in LB plus or minus CP or $ZnCl_2$ and grown for 6–7 h. Cultures were pelleted at 4 °C and then air dried on ice. RNA preparation and qRT-PCR was performed as described previously (Mortensen et al., 2014). See Supplemental Experimental Procedures.

GTPase activity assays

GTPase activity was measured by Malachite green assay (Attin et al., 2005). Briefly, purified ZigA (see Supplemental Experimental Procedures) was incubated with 0–1 mM GTP in assay buffer (150 mM NaCl, 20 mM Tris-HCl, pH 8.0, 2 mM $MgCl_2$) in a volume of 90 μL. After 90 min, 35 μL of Malachite green mixture (1.2 mL 0.045% Malachite green in 4 N HCl (Fluka), 400 μL 7.5% ammonium molybdate (Aldrich) and 25.6 μL 11% TWEEN-20 in 4 N HCl) was added, incubated for 3 min, and reaction stopped by addition of 15 μL 35% citric acid (Sigma) in 4 N HCl. After 30 min, the absorbance at 680 nm was correlated to the concentration of free phosphate using a standard curve (Fluka).

Mf2 Zn competition assays

Experiments were performed as described previously using an ISS PC1 spectrofluorimeter at 25 °C (Campanello et al., 2013; Reyes-Caballero et al., 2010). For mf2 titrations, λ_{ex}= 333 nm or 378 nm while λ_{em}= 505 nm. ≈5 μM protomer and 2 μM mf2 in 2 mL were incubated for 10 min in chelexed buffer (25 mM HEPES, 150 mM NaCl, 3 mM TCEP, pH 7.4) and aliquots of 1 mM $ZnSO_4$ were added. Equilibrium time was 2–5 min between measurements. Peak intensities at 333 and 378 nm from two or more experiments were globally fit to 2:1 binding models (mf2) with K_{Zn}^{mf2} fixed to their known values using Dynafit (Kuzmic, 1996). The same approach was used for determining Zn binding affinities of *L*-His and urocanic acid.

HAL activity assays

0.5~2 μM purified HutH (see Supplemental Experimental Procedures) was incubated with various concentrations of *L*-His (Sigma) (25 mM HEPES, 100 mM KCl, 3 mM TCEP, pH 7.5, with Zn or chelator) for 3 min at ambient temperature. Reactions were quenched with 3-fold HPLC running buffer A (2% MeOH, 98% water, 0.1% TFA). Samples were run though a spin column to remove proteins and injected onto a Kinetex C18 reverse phased column (Phenomenex XB-C18 100 Å) on a Waters 600 HPLC system equipped with a Waters 717 plus auto-sampler and Waters 486 tunable absorbance detector. Following injection, the HPLC was run as follows: 0–5 min 0% buffer B (95% MeOH, 5% water, 0.1% TFA), 5–15 gradient to 100% buffer B, 15–18 min, 100% buffer B, 18–20 min gradient to 0% buffer B. Urocanic acid was detected by absorbance at 277 nm with concentration determined from the integrated peak areas by comparison to a standard curve of urocanic acid (Aldrich).

Inductively-coupled plasma mass spectrometry

Purified ZigA or HutH was diluted to 1 mg/mL in 1 mL 20 mM Tris-HCl, pH 7.5, 150 mM NaCl in metal-free tubes (VWR) and diluted to 10 mL with diH_2O. For bacteria, strains were grown in CP as previously described for 6–7 h. Samples were normalized to the same OD_{600} and confirmed by CFU enumeration. Cells were pelleted at 4 °C, washed twice with diH_2O, incubated overnight in 50% nitric acid at 50 °C in metal-free tubes, and volume adjusted to 10 mL with diH_2O. Elemental quantification was performed on a Perkin-Elmer Elan DRCII ICP-MS equipped with AS-93 autosampler or a Thermo Fisher Scientific Element 2 ICP-MS coupled with ESI autosampler (Elemental Scientific).

Analytical gel filtration chromatography

A Superdex™ 200 increase 10/300 GL column was run in buffer D (25 mM HEPES, 150 mM NaCl, 5 mM TCEP, pH 7.4) at a flow-rate of 0.5 mL/min and calibrated with the Gel Filtration Calibration Kit HMW (GE Healthcare). A linear fit a plot of K_{av} vs. log M_r gave R^2= 0.99. 30 μM protein was incubated with ligands, *e.g.*, Zn, GTP, and/or GDP, on ice for 1 h, and 100 μL sample injected.

His mass spectrometry

WT and mutant bacteria were grown in the presence of 250 μg/mL CP or 500 μM $ZnCl_2$ all in LB plus CP buffer and grown for 8 h. Samples were normalized to the same OD_{600}, which was confirmed by dilution plating for CFUs. Cultures were centrifuged for 10 min at 4 °C. Bacteria were lysed as described above. Supernatants were mixed with 2:1 with methanol to which was added 10 μL of 2.5 μM stock of deuterated *L*-His-d_3 (α-d_1:imidazole-2,5-d_2) (C/D/N Isotopes). After 5 min, debris was removed by centrifugation at 10,000 × *g* for 5 min. Supernatant was loaded onto a spin filter with a 3000 D MWCO (Millipore) and centrifuged at 10,000 × *g* for 45 min to remove proteins. Samples were dansylated and mass spectrometry analyses were carried out using a standard of known *L*-His concentrations. See Supplemental Experimental Procedures.

His-Zn uptake assay

Overnight cultures of bacteria were diluted 1:50 in LB and grown at 37 °C for 1 h. These cultures were re-seeded 1:100 in 10 mL CP media plus or minus 150 μg/mL CP for 6 h. Cells were normalized to the same OD_{600}, pelleted, and suspended in 1 mL 50 mM Tris-HCl, pH 7.5, 1 mM $MgCl_2$. His-Zn complexes were prepared by incubating 1 mM *L*-His (Sigma) and 500 μM Zn^{70} or 500 μM Zn^{70} alone in 5 mL of 50 mM Tris-HCl, pH 7.5 for 30 min. Buffer only, Zn^{70}, or His-Zn complexes were diluted 1:10 into the bacterial samples and incubated for 30 min. Uptake was quenched with 1 mL ice cold ethanol:acetone (1:1) and incubated 10 min on ice. Cells were pelleted and washed twice with Milli-Q water. Samples were then suspended in 0.5 mL Milli-Q water and 1 mL of 50% Optima Ultra-pure nitric acid (Fisher), incubated overnight at 50 °C, and then diluted in Milli-Q water to 10 mL. ICP-MS was performed on a Perkin-Elmer DRCII ICP-MS equipped with AS-93 autosampler and DRC cell as outlined in our previous work (Jacobsen et al., 2011).

Supplementary Material

Refer to Web version on PubMed Central for supplementary material.

Acknowledgments

Work presented in this manuscript was supported by grants R01 AI1091771, R01 AI101171, and R01 GM042569 from the NIH. B.L.N. was supported by grant F32 AI108192 from the NIAID and the Childhood Infection Research Program T32 AI095202. Z.R.L. is supported by the Training Program in Environmental Toxicology T32 ES007028. V.d.C-L. is supported by the grant R01 GM70641 from the NIH. The content of this article does not necessarily represent the views of the NIH or NIAID and is solely the responsibility of the authors.

References

Andreini C, Banci L, Bertini I, Rosato A. Zinc through the three domains of life. J. Proteome Res. 2006; 5:3173–3178. [PubMed: 17081069]

Attin T, Becker K, Hannig C, Buchalla W, Wiegand A. Suitability of a malachite green procedure to detect minimal amounts of phosphate dissolved in acidic solutions. Clin. Oral Investig. 2005; 9:203–207.

Bender RA. Regulation of the histidine utilization (*hut*) system in bacteria. Microbiol. Mol. Biol. R. 2012; 76:565–584.

Blaby-Haas CE, Flood JA, Crecy-Lagard V, Zamble DB. YeiR: a metal-binding GTPase from *Escherichia coli* involved in metal homeostasis. Metallomics. 2012; 4:488–497. [PubMed: 22511334]

Bruins MR, Kapil S, Oehme FW. Microbial resistance to metals in the environment. Ecotoxicol. Environ. Saf. 2000; 45:198–207. [PubMed: 10702338]

Campanello GC, Ma Z, Grossoehme NE, Guerra AJ, Ward BP, Dimarchi RD, Ye Y, Dann CE 3rd, Giedroc DP. Allosteric inhibition of a zinc-sensing transcriptional repressor: insights into the arsenic repressor (ArsR) family. J. Mol. Biol. 2013; 425:1143–1157. [PubMed: 23353829]

Cavet, JS.; Perry, RD.; Brunke, S.; Darwin, KH.; Fierke, CA.; Imlay, JA.; Murphy, MEP.; Schryvers, AB.; Thiele, DJ.; Weiser, JN. Trace Metals in Host-Microbe Interactions: The Microbe Perspective. In: Skaar, EP.; Nriagu, JO., editors. Trace Metals and Infectious Disease. Cambridge, MA: The MIT Press; 2015. p. 99-124.

Colvin RA, Holmes WR, Fontaine CP, Maret W. Cytosolic zinc buffering and muffling: their role in intracellular zinc homeostasis. Metallomics. 2010; 2:306–317. [PubMed: 21069178]

Corbin BD, Seeley EH, Raab A, Feldmann J, Miller MR, Torres VJ, Anderson KL, Dattilo BM, Dunman PM, Gerads R, et al. Metal chelation and inhibition of bacterial growth in tissue abscesses. Science. 2008; 319:962–965. [PubMed: 18276893]

Doyle JS, Buising KL, Thursky KA, Worth LJ, Richards MJ. Epidemiology of infections acquired in intensive care units. Sem. Resp. Crit. Care Med. 2011; 32:115–138.

Gabriel SE, Miyagi F, Gaballa A, Helmann JD. Regulation of the *Bacillus subtilis yciC* gene and insights into the DNA-binding specificity of the zinc-sensing metalloregulator Zur. J. Bacteriol. 2008; 190:3482–3488. [PubMed: 18344368]

Haas CE, Rodionov DA, Kropat J, Malasarn D, Merchant SS, de Crecy-Lagard V. A subset of the diverse COG0523 family of putative metal chaperones is linked to zinc homeostasis in all kingdoms of life. BMC Genomics. 2009; 10:470. [PubMed: 19822009]

Haley KP, Delgado AG, Piazuelo MB, Mortensen BL, Correa P, Damo SM, Chazin WJ, Skaar EP, Gaddy JA. The Human Antimicrobial Protein Calgranulin C Participates in Control of *Helicobacter pylori* Growth and Regulation of Virulence. Infect. Immun. 2015; 83:2944–2956. [PubMed: 25964473]

Helbig K, Bleuel C, Krauss GJ, Nies DH. Glutathione and transition-metal homeostasis in *Escherichia coli*. J. Bacteriol. 2008; 190:5431–5438. [PubMed: 18539744]

Hood MI, Mortensen BL, Moore JL, Zhang Y, Kehl-Fie TE, Sugitani N, Chazin WJ, Caprioli RM, Skaar EP. Identification of an *Acinetobacter baumannii* zinc acquisition system that facilitates

resistance to calprotectin-mediated zinc sequestration. PLoS Pathog. 2012; 8:e1003068. [PubMed: 23236280]

Hood MI, Skaar EP. Nutritional immunity: transition metals at the pathogen-host interface. Nature Rev. Microbiol. 2012; 10:525–537. [PubMed: 22796883]

Horn NM, Thomas AL, Tompkins JD. The effect of histidine and cysteine on zinc influx into rat and human erythrocytes. J. Physiol. 1995; 489:73–80. [PubMed: 8583417]

Imlay, JA. Common Mechanisms of Bacterial Metal Homeostasis. In: Skaar, EP.; Nriagu, JO., editors. Trace Metals and Infectious Disease. Cambridge, MA: The MIT Press; 2015. p. 57-82.

Jacobsen FE, Kazmierczak KM, Lisher JP, Winkler ME, Giedroc DP. Interplay between manganese and zinc homeostasis in the human pathogen *Streptococcus pneumoniae*. Metallomics. 2011; 3:38–41. [PubMed: 21275153]

Klee CB. Metal activation of histidine ammonia-lyase. Metal ion-sulfhydryl group relationship. J. Biol. Chem. 1972; 247:1398–1406. [PubMed: 4622230]

Kuzmic P. Program DYNAFIT for the analysis of enzyme kinetic data: application to HIV proteinase. Anal. Biochem. 1996; 237:260–273. [PubMed: 8660575]

Loutet, SA.; Chan, ACK.; Kobylarz, MJ.; Verstraete, MM.; Pfaffen, S.; Ye, B.; Arrieta, AL.; Murphy, MEP. The Fate of Intracellular Metal Ions in Microbes. In: Skaar, EP.; Nriagu, JO., editors. Trace Metals and Infectious Disease. Cambridge, MA: The MIT Press; 2015. p. 39-56.

Ma Z, Chandrangsu P, Helmann TC, Romsang A, Gaballa A, Helmann JD. Bacillithiol is a major buffer of the labile zinc pool in *Bacillus subtilis*. Mol. Microbiol. 2014; 94:756–770. [PubMed: 25213752]

Maier T, Jacobi A, Sauter M, Bock A. The product of the *hypB* gene, which is required for nickel incorporation into hydrogenases, is a novel guanine nucleotide-binding protein. J. Bacteriol. 1993; 175:630–635. [PubMed: 8423137]

Mortensen BL, Rathi S, Chazin WJ, Skaar EP. *Acinetobacter baumannii* response to host-mediated zinc limitation requires the transcriptional regulator Zur. J. Bacteriol. 2014; 196:2616–2626. [PubMed: 24816603]

Murphy JT, Bruinsma JJ, Schneider DL, Collier S, Guthrie J, Chinwalla A, Robertson JD, Mardis ER, Kornfeld K. Histidine protects against zinc and nickel toxicity in *Caenorhabditis elegans*. PLoS Genetics. 2011; 7:e1002013. [PubMed: 21455490]

Padovani D, Banerjee R. A G-protein editor gates coenzyme B12 loading and is corrupted in methylmalonic aciduria. Proc. Natl. Acad. Sci. 2009; 106:21567–21572. [PubMed: 19955418]

Palacios O, Atrian S, Capdevila M. Zn- and Cu-thioneins: a functional classification for metallothioneins? J. Biol. Inorg. Chem. 2011; 16:991–1009. [PubMed: 21823038]

Reyes-Caballero H, Guerra AJ, Jacobsen FE, Kazmierczak KM, Cowart D, Koppolu UM, Scott RA, Winkler ME, Giedroc DP. The metalloregulatory zinc site in *Streptococcus pneumoniae* AdcR, a zinc-activated MarR family repressor. J. Mol. Biol. 2010; 403:197–216. [PubMed: 20804771]

Simm C, Lahner B, Salt D, LeFurgey A, Ingram P, Yandell B, Eide DJ. *Saccharomyces cerevisiae* vacuole in zinc storage and intracellular zinc distribution. Eukaryot. Cell. 2007; 6:1166–1177. [PubMed: 17526722]

Soriano A, Colpas GJ, Hausinger RP. UreE stimulation of GTP-dependent urease activation in the UreD-UreF-UreG-urease apoprotein complex. Biochemistry. 2000; 39:12435–12440. [PubMed: 11015224]

Sydor AM, Jost M, Ryan KS, Turo KE, Douglas CD, Drennan CL, Zamble DB. Metal binding properties of *Escherichia coli* YjiA, a member of the metal homeostasis-associated COG0523 family of GTPases. Biochemistry. 2013; 52:1788–1801. [PubMed: 24449932]

Sydor AM, Liu J, Zamble DB. Effects of metal on the biochemical properties of *Helicobacter pylori* HypB, a maturation factor of [NiFe]-hydrogenase and urease. J. Bacteriol. 2011; 193:1359–1368. [PubMed: 21239585]

VanZile ML, Chen X, Giedroc DP. Structural characterization of distinct alpha3N and alpha5 metal sites in the cyanobacterial zinc sensor SmtB. Biochemistry. 2002; 41:9765–9775. [PubMed: 12146942]

Vishniac HS. The nutritional requirements of isolates of *Labyrinthula spp*. J. Gen. Microbiol. 1955; 12:455–463. [PubMed: 14392300]

Waldron KJ, Rutherford JC, Ford D, Robinson NJ. Metalloproteins and metal sensing. Nature. 2009; 460:823–830. [PubMed: 19675642]

Zambelli B, Stola M, Musiani F, De Vriendt K, Samyn B, Devreese B, Van Beeumen J, Turano P, Dikiy A, Bryant DA, et al. UreG, a chaperone in the urease assembly process, is an intrinsically unstructured GTPase that specifically binds Zn^{2+} . J. Biol. Chem. 2005; 280:4684–4695. [PubMed: 15542602]

Zhang XX, Rainey PB. Genetic analysis of the histidine utilization (*hut*) genes in *Pseudomonas fluorescens* SBW25. Genetics. 2007; 176:2165–2176. [PubMed: 17717196]

Zhou L, Li S, Su Y, Yi X, Zheng A, Deng F. Interaction between histidine and Zn(II) metal ions over a wide pH as revealed by solid-state NMR spectroscopy and DFT calculations. J. Phys. Chem. B. 2013; 117:8954–8965. [PubMed: 23841698]

Highlights

- *A. baumannii* responds to Zn starvation by up-regulating a Zn metallochaperone ZigA
- ZigA is a Zn-binding GTPase that impacts intracellular histidine levels in low Zn
- The histidine ammonia-lyase HutH is activated by Zn, potentially obtained from ZigA
- Histidine is a labile Zn pool mobilized during low Zn via histidine degradation by HutH

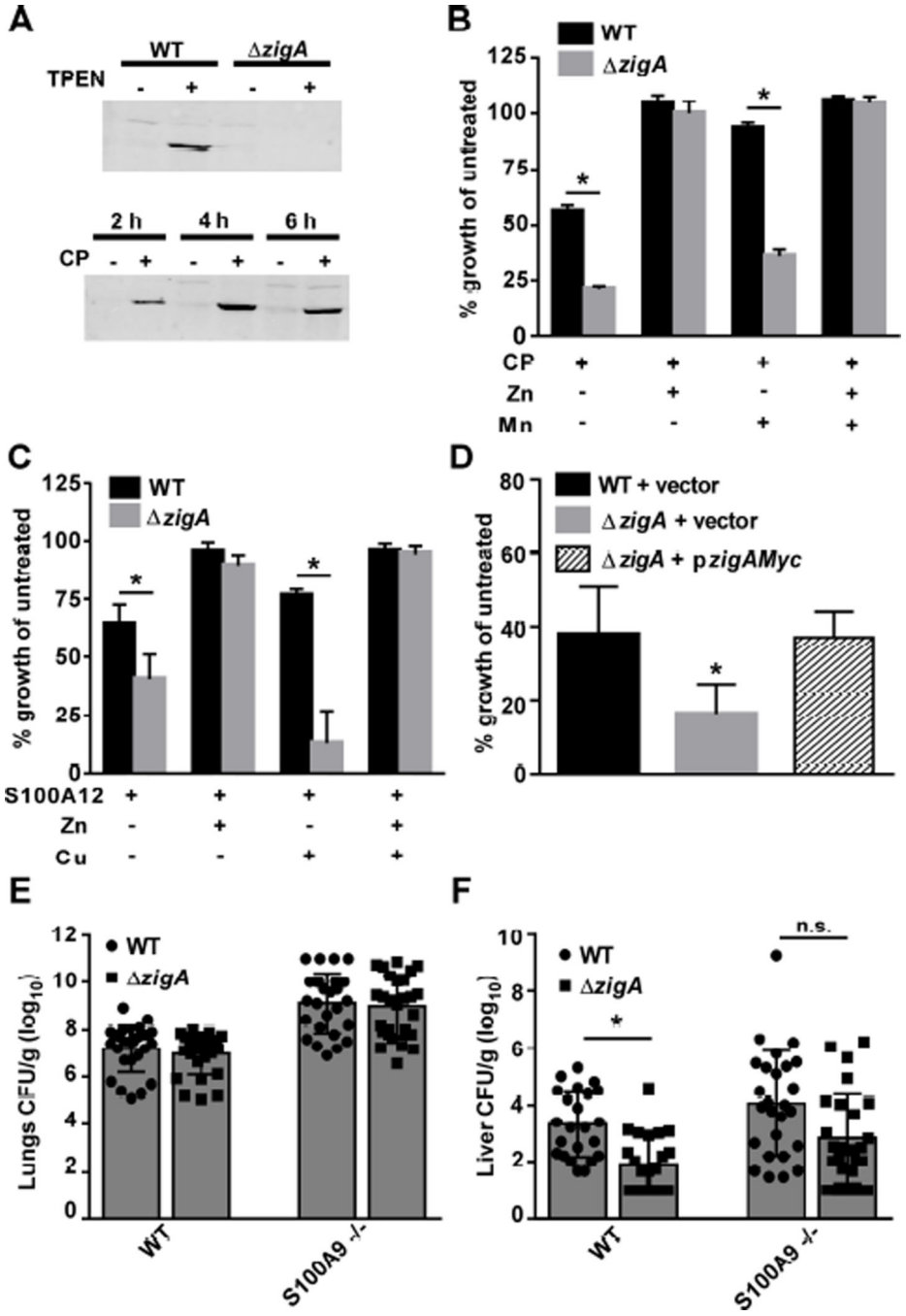

Figure 1. ZigA is required for full growth in low Zn and during infection

(A) ZigA protein expression was assessed in WT and Δ*zigA* in LB or LB plus 20 μM TPEN or in 250 μg/mL CP. (B) WT or Δ*zigA* were grown in the absence or presence of 250 μg/mL CP plus or minus Zn or Mn. Graph depicts % growth at 8 h. *$p < 0.0001$ as determined by Student's *t* test. (C) WT or Δ*zigA* were grown in the absence or presence of 500 μg/mL S100A12 plus or minus Zn or Cu. Graph depicts % growth at 8 h. *$p < 0.05$ as determined by Student's *t* test. (D) Growth of WT + vector, Δ*zigA* + vector, and Δ*zigA* + *pzigAMyc* was monitored in LB or LB plus 40 μM TPEN. Graph depicts % growth at 8 h. *$p < 0.05$ as

determined by Student's *t* test. (E, F) WT or S100A9$^{-/-}$ mice were infected intranasally with WT and Δ*zigA* in a competition experiment. At 36 h, lungs (E) and livers (F) were removed, homogenized, and CFU were enumerated. *$p < 0.05$ as determined by Kruskal-Wallis with Dunn's multiple comparisons (see Figure S1).

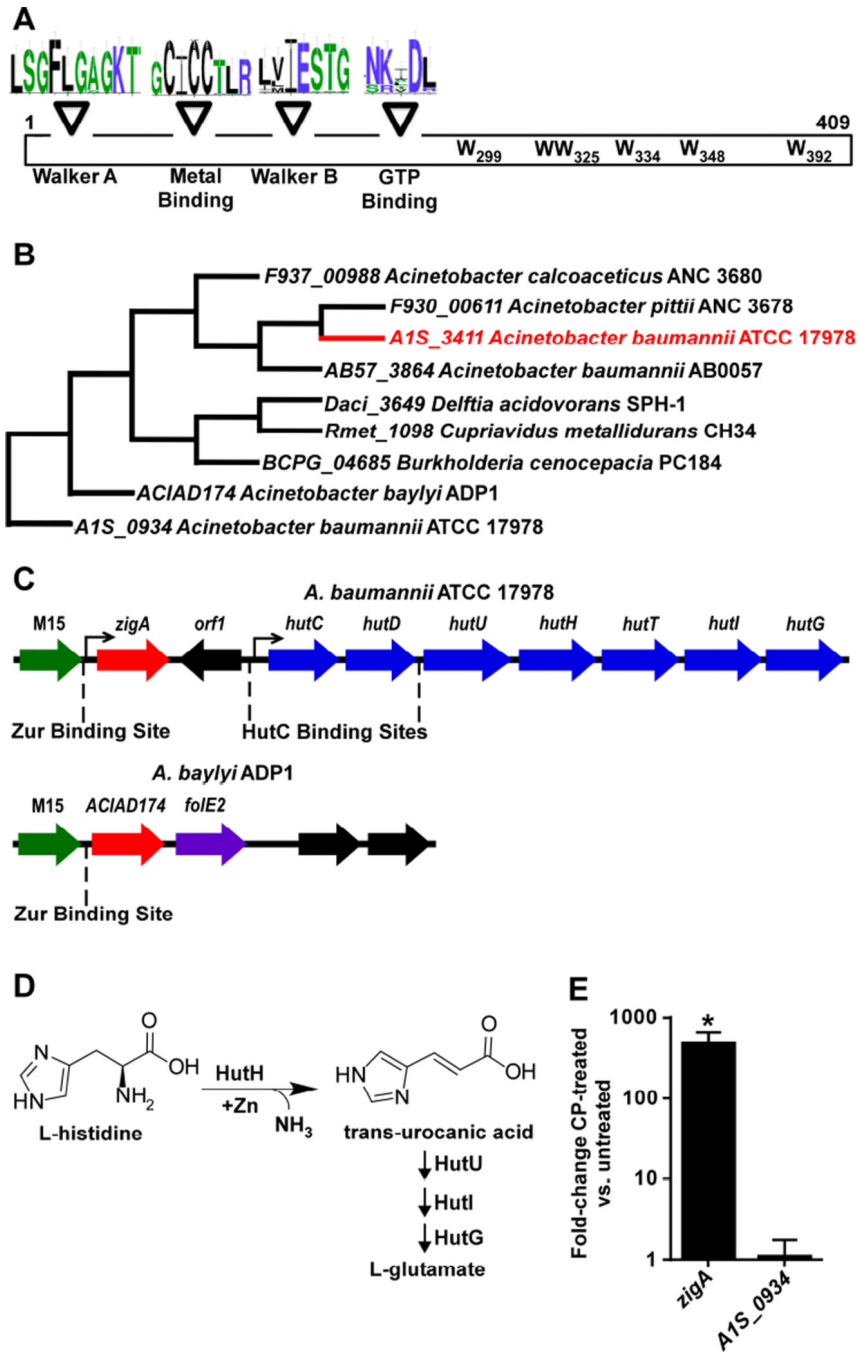

Figure 2. ZigA is a COG0523 group 1 member that clusters with the *hut* operon

(A) Conserved residues and motifs of the ZigA subfamily; positions correspond to the ZigA sequence numbering. (B) A subset of the COG0523 group 1 sequences with the addition of the paralog from another COG0523 subgroup found in *A. baumannii* (A1S_0934) were used to generate a phylogenetic tree; clustering with the *hut* operon or *folE2* encoding a non-Zn requiring paralog of GTP cyclohydrolase, GTP cyclohydrolase 1b, is noted. (C) Gene neighborhoods of ZigA in two *A. baumannii* species and in *A. baylyi* ADP1 showing the positions of the Zur and HutC binding site in *A. baumannii* AB0057. (D) Enzymatic

pathway of His degradation. (E) Expression of *zigA* and *A1S_0934* in CP-treated *A. baumannii* as assessed by qRT-PCR. * $p < 0.05$ as determined by Student's *t* test.

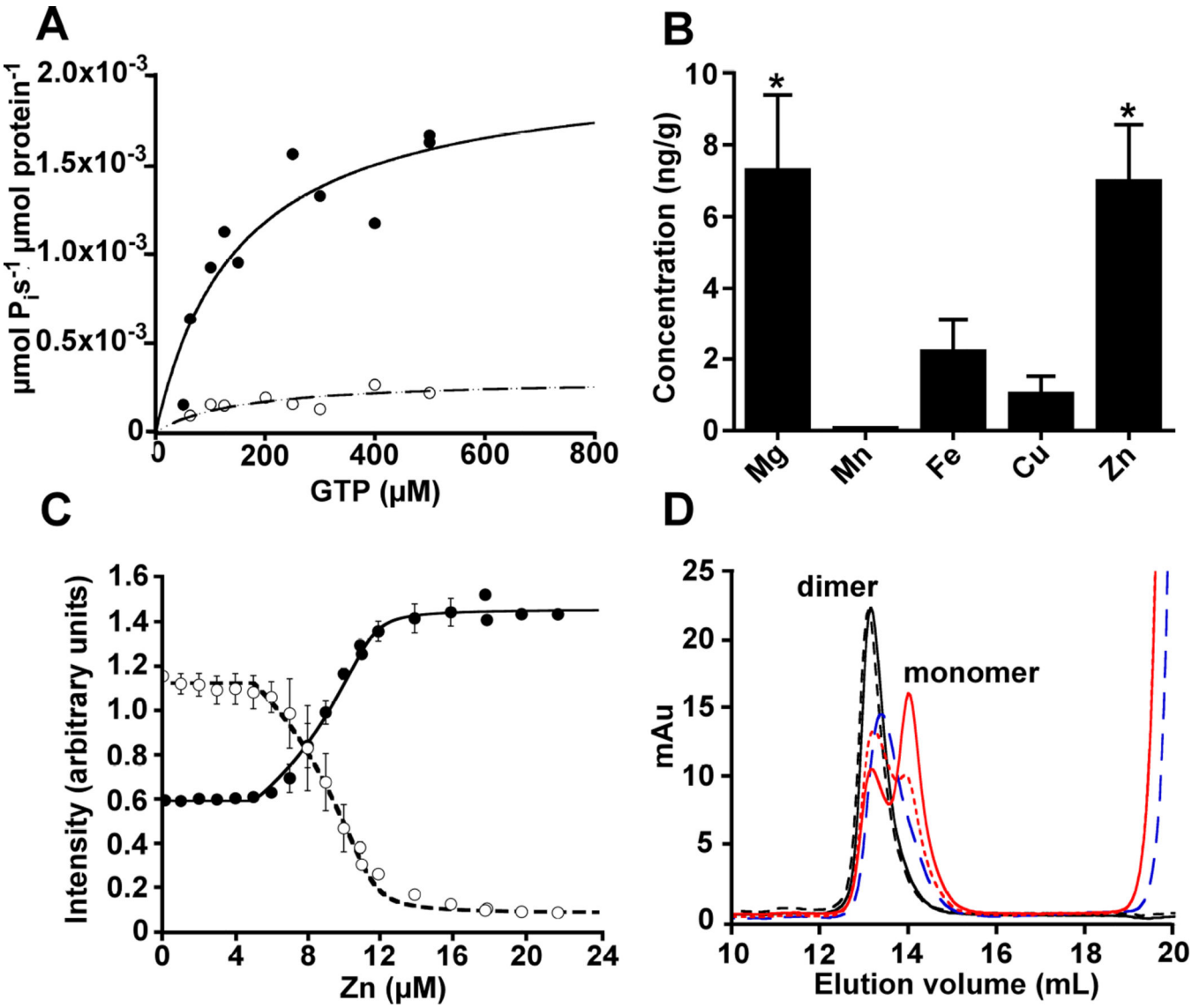

Figure 3. ZigA is a Mg- and Zn-binding GTPase

(A) Zn-bound ZigA (closed circles) or apo-ZigA (with 0.1 mM TPEN (open circles)) (2 µM) was incubated with the indicated [GTP] for 1.5 h (see Figure S2), followed by quantitation of the released inorganic phosphate (P_i). The continuous lines through the data are fits to the Michaelis–Menten equation. For Zn-bound-ZigA, K_m (GTP) = 150 (± 60) µM, k_{cat} = 2.1 (± 0.3) × 10^{-3} s^{-1}. For apo-ZigA, k_{cat} = 3.0 (±0.2) × 10^{-4} s^{-1} with K_m constrained to the value for Zn-ZigA. (B) Recombinant ZigA was analyzed by ICP-MS for associated Mg, Mn, Fe, Cu, and Zn concentrations. *$p < 0.05$ as determined by one-way ANOVA. (C) Duplicate binding isotherms (mean and range shown for each data point) obtained from titrating Zn into a mixture of metal-free apo-ZigA (5.0 µM protomer) and mf2 (2.0 µM) competitor. *Filled* symbols, emission intensity with excitation at 333 nm; *open* symbols, excitation at 378 nm. The continuous line represents a global non-linear, least-squares fit to a 2:1 Zn:ZigA protomer model, with $K_{Zn1} \geq 10$ M^{-1} (lower limit) and K_{Zn2} = 2.6 (±0.4) × 10 M^{-1}. (D) ZigA was subjected to chromatography on Sephadex G200 in the apo-state (*black*, *solid*

line); + 2.0 protomer mol•equiv of Zn (*black*, *dashed*); + 2.0 protomer mol•equiv of Zn + 3 mM Mg^{2+}•GDP (*blue*, *long-dash*); + 3 mM Mg^{2+}•GDPNP (*red, dashed* line); + 2.0 protomer mol•equiv of Zn + 3 mM Mg^{2+}•GDPNP (*red*, *solid*). The absorbance at 19 mL corresponds to added nucleotide (defines the included volume). *Dimer:* 100 kDa measured (92.8 kDa expected); *monomer:* 64 kDa measured (46.4 kDa expected).

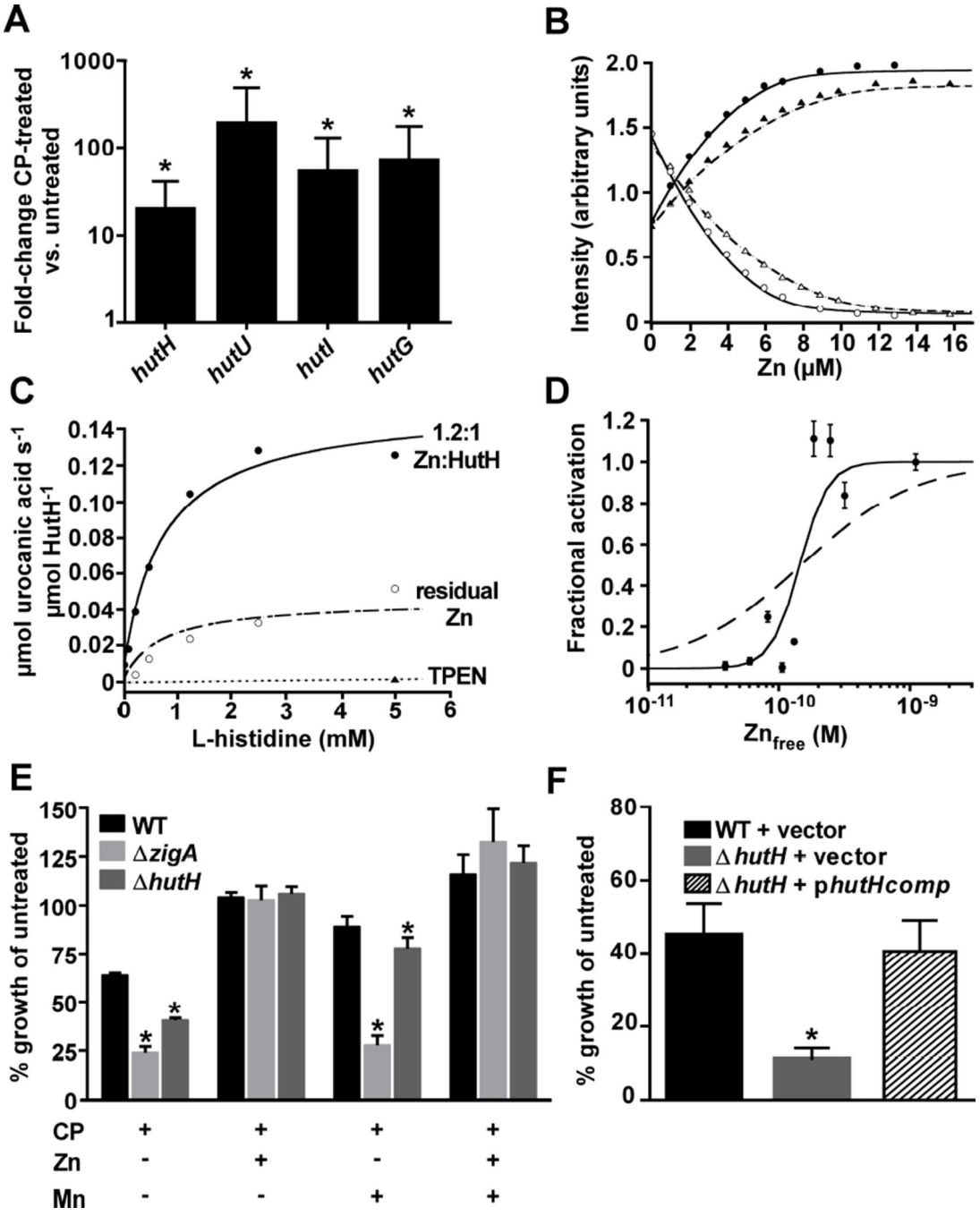

Figure 4. HutH binds Zn and is important for growth in low Zn conditions

(A) Gene expression of *hutH, hutU, hutI,* and *hutG* in CP-treated *A. baumannii* as assessed by qRT-PCR. **p*<0.05 as determined by Student's *t* test. (B) Representative binding isotherms obtained from titrating Zn into a mixture of apo-HutH (5.1 μM, circles; 8.5 μM, triangles) and mf2 (2.0 μM) competitor. *Filled* symbols, emission intensity with excitation at 333 nm; *open* symbols, excitation at 378 nm. The continuous line represents a global non-linear, least-squares fit to a 1:1 Zn:ZigA protomer model, with K_{Zn1}= 5.0 (± 0.2) × 10 M^{-1}. (C) HAL activity was measured using an LC-based assay to detect urocanic acid. HAL

activity (0.5 μM HutH) as a function of *L*-His in the presence of saturating Zn (*filled* circles); residual Zn (0.1 μM) in the assay buffer (*open* circles); in the presence of 0.15 mM TPEN (*closed* triangles). The continuous lines through the data points represent a fit to the Michaelis-Menten equation with the optimized: K_m*=0.7* (±0.1) mM, with maximal velocities, V_{max}=0.15 (±0.01) s^{-1} for Zn-saturated HutH and 0.045 (±006) s^{-1} for residual Zn. (D) HutH (0.5 μM) HAL specific activity (k_{cat}, s^{-1}) was measured at excess total Zn, but with varying $[Zn]_{free}$, buffered with 0.25 mM EGTA at 5.0 mM *L*-His (≈8-fold over the K_m). The continuous line through the data represent a fit to a simple cooperative Hill binding model with n_H=4 leading to ≈30-fold activation by Zn (k_{cat}: 0.16 (+/−0.01) s^{-1} (+Zn); k_{cat}: 6.0 (+/−3.0) × 10^{-3} s^{-1} (–Zn)). K_{Zn} for HutH activation is 8.5 × 10^9 M^{-1}*Dashed line*, fit to a non-cooperative Zn-activation model. (E) WT, Δ*zigA*, and Δ*hutH* were grown in the absence or presence of 250 μg/mL CP plus or minus Zn or Mn. Graph depicts % growth at 8 h. **p*<0.05 as determined by two-way ANOVA. (F) WT + vector, Δ*hutH* + vector, and Δ*hutH* + p*hutHcomp* were grown in the absence or presence of 40 μM TPEN. The graph depicts % growth at 8 h. **p* < 0.05 as determined by Student's *t* test (see Figures S3–S4).

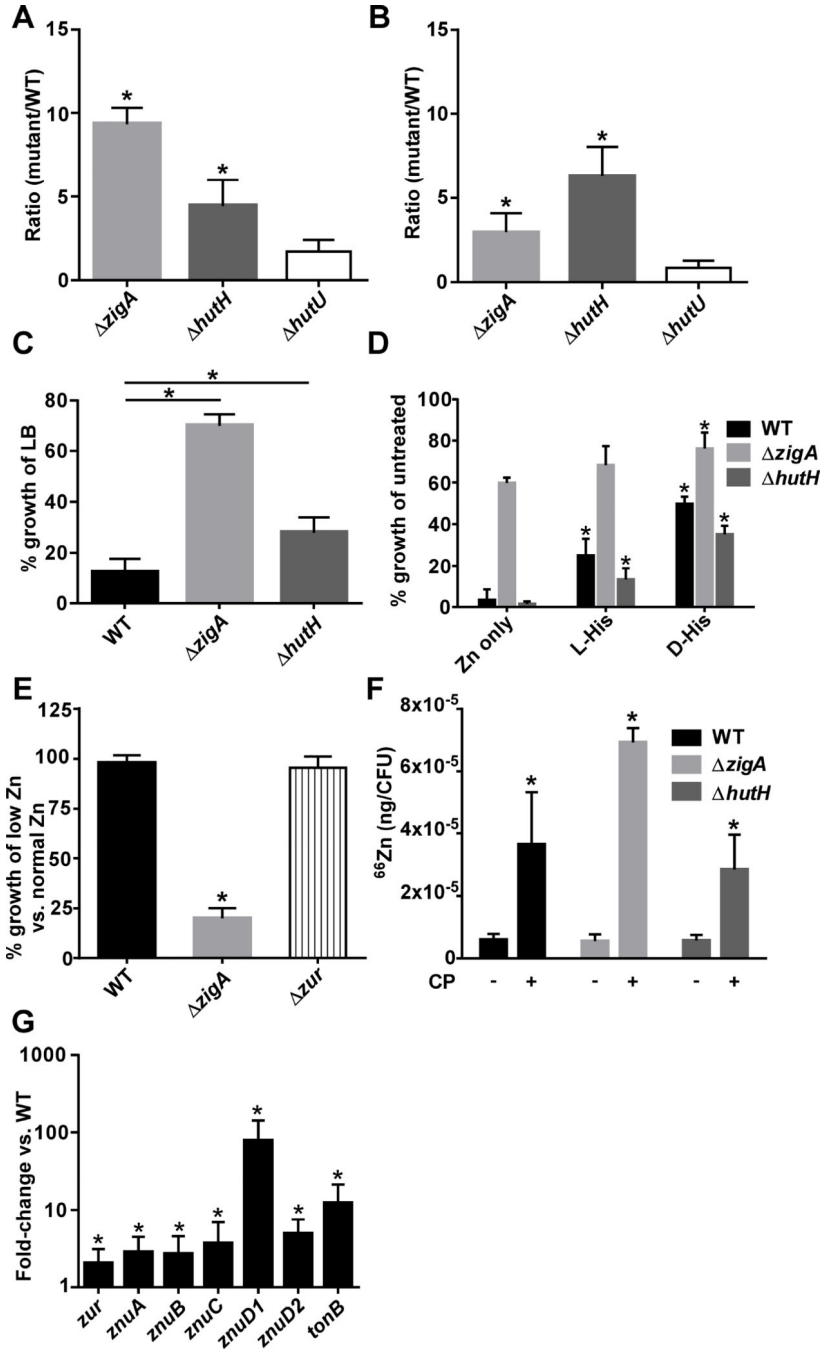

Figure 5. ZigA and HutH impact a His-Zn pool

(A, B) WT, Δ*zigA*, Δ*hutH*, and Δ*hutU* were grown the presence of (A) 250 μg/mL CP or (B) 500 μM $ZnCl_2$, and intracellular His levels were assessed by mass spectrometry. *$p < 0.05$ as determined by Student's *t* test. (C) WT, Δ*zigA*, and Δ*hutH* were grown in LB or LB plus 1.25 mM $ZnCl_2$, depicted as % growth at 12 h. *$p < 0.0001$ as determined by Student's *t* test. (D) WT, Δ*zigA*, and Δ*hutH* were grown in LB plus 1.25 mM $ZnCl_2$ and 1 mM of *L*-His or *D*-His were added to the cultures. Graph depicts % growth of each strain in the treated condition compared to LB at 8 h. (E) WT, Δ*zigA*, and Δ*zur* were grown in M9 media with

50 mM His as a sole carbon source in Zn replete or deplete (no Zn added) conditions. *$p <$ 0.05 as determined by two-way ANOVA. (F) Intracellular Zn levels in WT, Δ*zigA*, and Δ*hutH* in CP-treated vs. untreated cells as measured by ICP-MS. *$p<0.05$ as determined by Student's *t* test. (G) Expression of Zur-regulated genes in Δ*zigA* in the absence of CP compared to WT as assessed by qRT-PCR. *$p<0.05$ as determined by Student's *t* test (see Figure S5).

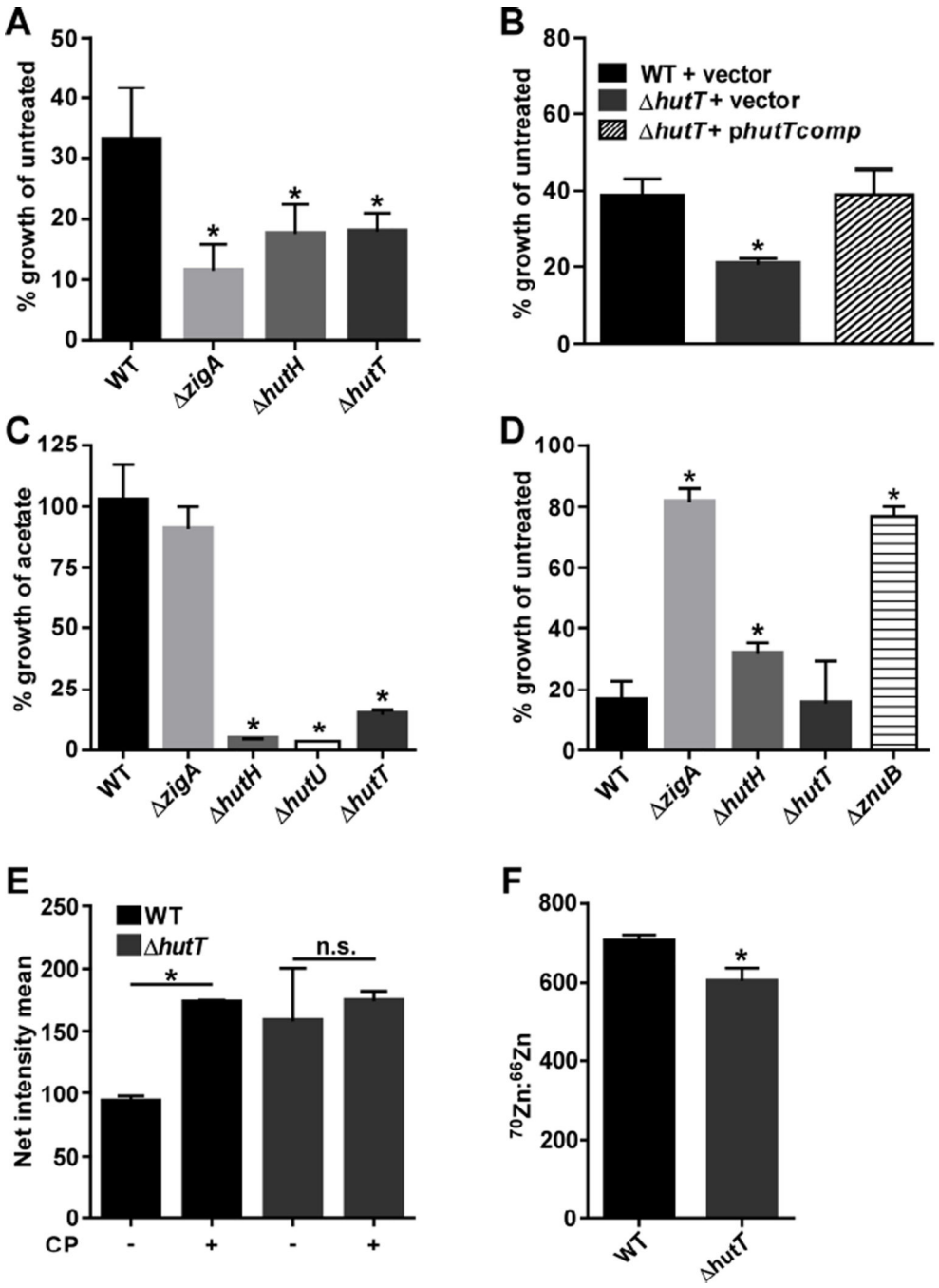

Figure 6. The His-Zn pool is affected by the HutT His importer

(A) WT, Δ*zigA*, Δ*hutH*, and Δ*hutT* were grown in the absence or presence of 250 μg/mL CP. Graph depicts % growth at 8 h. *$p < 0.05$ as determined by two-way ANOVA. (B) WT + vector, Δ*hutT* + vector, and Δ*hutT* + p*hutTcomp* were grown in the absence or presence of 40 μM TPEN. Graph depicts growth at 8 h. *$p < 0.05$ as determined by Student's *t* test. (C) WT, Δ*zigA*, Δ*hutH*, Δ*hutU*, and Δ*hutT* were grown in M9 media with a titration of His or acetate as a sole carbon source. *$p < 0.05$ as determined by Student's *t* test. (D) WT, Δ*zigA*, Δ*hutH*, Δ*hutT*, and Δ*znuB* were grown in LB or LB plus 1.25 mM $ZnCl_2$. Graph displays %

growth at 12 h. *$p < 0.0001$ as determined by Student's *t* test. (E) Zn uptake was evaluated following growth plus or minus CP for WT or Δ*hutT* after 30 min incubation with Zn^{70}, and ICP-MS analysis of intracellular Zn^{70} shown as net intensity mean. *$p < 0.05$ as determined by Student's *t* test. (F) Uptake of His-Zn complexes in CP-treated cells was assessed for WT and Δ*hutT* incubated for 30 min with Zn^{70}-His complexes and the intracellular Zn^{70}:Zn^{66} ratio measured by ICP-MS. *$p < 0.05$ as determined by Student's *t* test (see Figure S6).